Nuclear reactions as a tool to investigate laser proton acceleration inside plastic and inorganic targets

A. YOUSSEF[a,c*] AND R. KODAMA[a,b]
[a]*Institute of Laser Engineering (ILE), Osaka University, 2-6 Suita, Osaka 565-0871, Japan*
[b]*Graduate School of Engineering, Osaka University, 2-1 Suita, Osaka 565-0871, Japan*
[c]*Physics Department, Faculty of Science, Sohag University, Sohag 82524, Egypt*

Nuclear reactions generated from ultra-intense laser interactions with plastic and inorganic targets have been used to investigate the proton acceleration process inside these targets. Nuclear reactions occur between accelerated protons and target bulk ions and hence the action of the electrostatic sheath on the rear side is excluded. Thus we can confirm form where the accelerated protons originate and by which mechanism(s) they are accelerated inside the target. From measured and calculated spectra, by 3D Monte Carlo code, the origin, the acceleration mechanism(s), the maximum energy, the total number, and the mean energy of the accelerated protons are investigated.

(Received January 7, 2014; Accepted March 14, 2014)

Keywords: Laser ion acceleration, Nuclear reactions

1. Introduction

Recently established ultraintense laser systems with high contrast and extreme intensity, where the frontier of maximum intensity is now pushed to about 10^{22} W/cm^2, provide a valuable tool for exploring new regimes in relativistic laser-plasma physics. The electromagnetic fields obtained at the laser focus drive electrons to relativistic momenta and as a result ion beams are accelerated to high energies. Laser ion acceleration is an active area for the combination of fundamental physics and technological progress. This combination has been opened the door for variety of applications that have recently become the matter of intensive studies. These applications are particularly in fast ignitor of laser fusion [1], radioisotope generation for medical purposes [2-4], material science [5], proton radiography of plasma [6], accelerator technology [7], and tabletop nuclear physics [8].

Right now, in spite of extensive studies, origins and the acceleration mechanisms of the accelerated ion are still a matter of discussion [9,10]. According to several studies, ions are generated and accelerated through the so called target normal sheath acceleration (TNSA) mechanism [11-13]. In TNSA mechanism, the ion beams are accelerated in vacuum at the rear surface of the target by the self-consistent electrostatic accelerating field generated by fast electrons accelerated at the irradiated surface by the laser ponderomotive force. Other studies indicated that ions are generated and accelerated inside the target at the front surface [14-16].

Particle in cell (PIC) simulations [17-19] and experimental observations [20,21] show that ions can be produced at the front and the rear sides simultaneously, even if the generation processes are quite different. Simulation by Emmanuel *et al.* [22], pointed out that the most energetic protons are first accelerated by an electrostatic shock at the front surface, cross the target, and gain additional energy from the TNSA. When these ions emerge at the rear surface, they are eventually accelerated to higher energy than the back-surface protons. Thus, both of the acceleration mechanisms will contribute in the acceleration process. Other simulation by Paul Gibbon [23] implied that the target resistivity leads to strong suprathermal heat-flow inhibition, even at intensities up to 10^{20} W cm^{-2}. This in turn radically alters the ion acceleration due to suppressing the sheath mechanism at the rear surface of the target and enhancing the shock-driven process at the front.

For plastic and inorganic targets, ponderomotive forces induced by a short laser pulse near the critical plasma surface drive dense plasma bunches (blocks) of ion densities comparable to (or higher than) the plasma critical density [24-27]. As these densities are about a thousand times higher than those produced by TNSA, even at moderate ion energies, the intensities and current densities of the driven ion beams can be extremely high, much higher than in the case of TNSA beams produced at comparable laser intensities and/or energies [24–25]. Producing of such protons will be of great benefit to many applications at high-energy-density physics. To investigate the acceleration mechanism(s) inside the target independently, a new tool to exclude the TNSA mechanism is needed. Thus not only the acceleration mechanism at the front surface but also across the target can be directly examined.

To date, ion acceleration measurement is usually made outside the target, and hence the origin of the ions and the acceleration mechanism(s) inside the target cannot be directly investigated. A more effective method to measure the ions inside the target is required. The energies of the accelerated ions lie significantly above the threshold

for nuclear reactions. For this reason nuclear reactions become a powerful tool for diagnosing these ions. Nuclear reactions that generated in laser-solid interactions occur between accelerated ions and target background ions inside the target. Accordingly, the action of TNSA mechanism is excluded and the ion acceleration mechanism(s) inside the target can be investigated independently. By analyzing the outgoing particles from the nuclear reactions, one can obtain knowledge on the accelerated ions inside the target. In this context, neutron producing reactions are unique probes. Because of their large mean free path and their neutral charge, neutrons readily carry information from inside the target without any effect due to electric and/or magnetic fields inside or around the target.

Some aspects about the front surface acceleration (FSA) were studied [28-31] from the interactions between ultra-intense lasers at intensities up to $2x10^{19}$ Wcm^{-2} and deuterated targets. The interpretation of the experimental results based on considering the $D(d,n)^3He$ reaction as the only productive reaction of the emitted neutron spectra. In previous studies[32-34], we pointed out that the $^{12}C(d,n)^{13}N$ and $D(^{12}c,n)\ ^{13}N$ reactions, which have much higher cross sections compared to the D-D reaction, strongly participate in the neutron yield. Also, we revealed that the neutron spectra produced by the D-C and C-D reactions can effectively overlap that produced by the D-D reaction especially when the intensity of the incident laser is higher than $3x10^{18}$ W/cm^2. In addition, neutron spectra produced by photonuclear reactions, deuteron break-up, deuteron electro-disintegration, and the reactions of protons, that contaminated the target surface, with D and C ions inside the target have to be taken into account. As a result, to substantiate any interpretations depending on neutron spectra produced from deuterated targets irradiated by ultra-intense lasers, all these neutron producing reactions have to be considered.

In this paper, we introduce a study that employs neutron spectra produced by the reaction $^7Li\ (p,n)^7Be$ to probe the origin, the acceleration mechanism(s), the maximum energy, the mean energy, and the total number of protons from the irradiated targets, LiF and CH-LiF. The reaction $^7Li\ (p,n)^7Be$ has a very high cross section (up to 600 mb) [35] and threshold energy of 1.88 MeV. In the case of LiF target, protons come from the hydrocarbon and/or water contaminations exist on the target surface. The CH-LiF target contains proton rich layer CH placed to check whether or not the neutron yield would increase by adding this layer. Thus we can confirm whether or not the ions originate from the front side.

2. Experimental work

The experiment performed using 30 TW Gekko MII short pulse ultraintense laser system at the Institute of Laser Engineering (ILE), Osaka University [36]. The 450 fs, 20-J, 1.053-μm, p-polarized laser at intensity of $3x10^{18}$ W/cm^2 was focused on LiF and CH-LiF targets. The incident angle of the p-polarized laser light was 20^0 relative to the target normal. The LiF layer is 500 μm in thickness to stop all the accelerated protons inside it whereas the thickness of the CH layer is 1.25 μm. Neutron detectors were positioned at 2.28 m from the target at angle 40^0 relative to the laser direction. Neutron diagnostics consisted of current mode time of flight (TOF) detectors comprised a scintillator/photomultiplier tube (PMT) combination. The scintillator type, ultra-fast timing plastic scintillator, is the quenched version of Bicron BC-422 scintillator (BC-422Q) with a decay time of 700 ps and a rise time of less than 20 ps [37]. The PMT, one of the highest performance timing tubes, is the Hamamatsu R2083 that has a rise time of 700 ps and a transit time spread of 370 ps. The detectors were shielded with 10 cm thick Pb wall placed in the front of the scintillator. In addition, detectors were protected by 5 cm of Pb plates on all sides. The modulation of the neutron spectra due to the shielding [38] was taken into account. Therefore, time of flight values of the neutron groups were corrected by considering the delay of the neutrons inside the lead blocks. The signal levels are normalized to the neutron yield per solid angle $d^2N/d\Omega$ dE (neutrons/MeV Sr), taking into account the detector position and sensitivity. The accuracy of each energy value is calculated by using the differentiation method [39]. According to this method, the error in neutron energy ΔE is calculated using the partial differentiation depending on the experimental errors in both time of flight ΔT and distance of the detector from the target ΔX as:

$$(\Delta E)^2 = (\partial E/\partial T)^2\ (\Delta T)^2\ + (\partial E/\partial X)^2\ (\Delta X)^2 \qquad (1)$$

To reduce the effect of the bremsstrahlung flashes, coming from the relativistic electrons interactions with both the instruments close to the target and the chamber wall, cone shaped collimator is installed in the chamber. The collimator limits the view of the detectors and reduces the bremsstrahlung flashes from the diagonal inner walls of the chamber. The body of the collimator was made of 1-Cm thick lead cylinder. To reduce bremsstrahlung on the collimator itself, the lead collimator was covered with 4.5 cm thick low z (plastic) electron moderate. The neutron detectors observe the target through a hole bored through the center of the electron moderator. Therefore, this low–z electron moderator also works as neutron collimator.

3. Discussion

Figs. 1&2 show the measured neutron spectra (black lines) observed from the irradiated targets, LiF and CH-LiF respectively. Neutrons with energies up to 1.27±0.08 MeV and 1.28±0.08 MeV emitted from the LiF and CH-LiF targets respectively. This means that the maximum energy of the emitted neutrons from the two targets is the same within the experimental error. In the experiment, the emitted neutrons is measured at angle $\theta=40^0$ relative to the laser direction. The laboratory energy of the emitted neutron E_b as a function of the incident proton energy E_a and the angle θ between the incident proton and the emitted neutron [40] is given as:

$$E_b^{1/2} = ((m_a m_b E_a)^{1/2} \cos\theta \pm \{m_a m_b E_a \cos^2\theta + (m_Y + m_b)[m_Y Q + (m_Y - m_a)E_a]\}^{1/2})/(m_Y + m_b) \quad (1)$$

where m_a, m_b, and m_Y are the masses of incident proton, emitted neutron, and produced nucleus respectively. From this formula, when the maximum energy of the emitted neutrons at $\theta=40^0$ is 1.28± 0.08 MeV, then the maximum energy of the incident protons is 3.1± 0.11 MeV. The maximum energy of the accelerated protons in the two cases is the same (within the experimental error). On the other hand, the neutron flux produced from the CH-LiF target (Fig.2) is more than twice that produced from the LiF one (Fig.1). Thus, the CH layer strongly increases the number of the accelerated protons but it does not affect the maximum acceleration energy. This indicates that the accelerated protons inside the target originate from the front side and propagate across the target producing neutrons through the ^{7}Li (p,n) ^{7}Be reaction with the target background ^{7}Li ions.

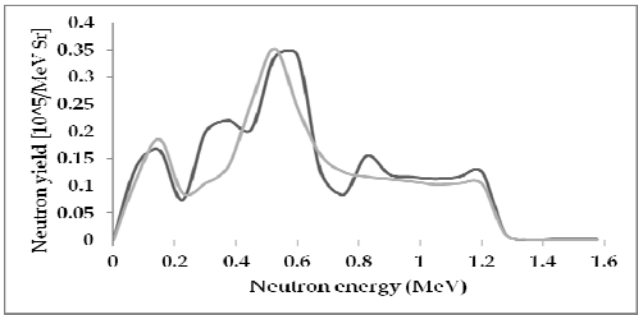

Fig. 1: The relation between the neutron energy E(θ) and the double differential neutron yield $d^2N/d\Omega\ dE$ (neutrons/MeV Sr) for neutron spectra from irradiated LiF target observed at 40^0 relative to the laser direction (black) compared with that produced from the 3-D Monte Carlo code (gray). The emitted neutrons have energies up to 1.27± 0.08 MeV.

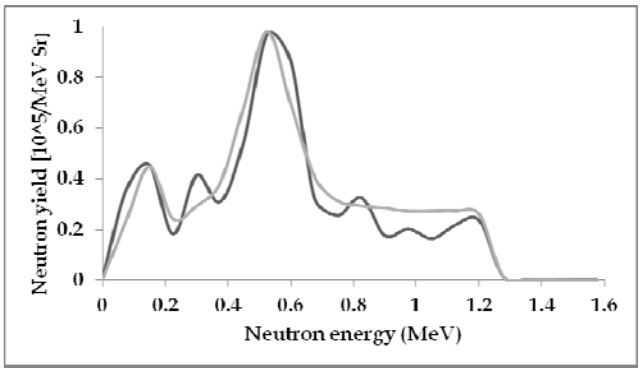

Fig. 2: The relation between the neutron energy E(θ) and the double differential neutron yield $d^2N/d\Omega\ dE$ (neutrons/MeV Sr) for neutron spectra from irradiated CH-LiF target observed at 40^0 relative to the laser direction (black) compared with that produced from the 3-D Monte Carlo code (gray). The emitted neutrons have energies up to 1.28± 0.08 MeV.

PIC Simulations [18, 19, 41, 42] suggest mechanisms that responsible for acceleration at the front surface. When the energy density of the laser wave greatly exceeds the kinetic energy of the plasma, the critical surface can be "pushed" inward, launching an ion shock wave. We can solve for the velocity of the ion wave by balancing the radiation pressure with the ion momentum flux in the frame of the reflection surface [41]. Only at the critical density n_c the laser starts to push ions forward and then the recession velocity u_s is expressed as [41]:

$$u_s/c = \sqrt{\tfrac{1}{2}\frac{n_e}{n_c}\frac{zm}{M}a^2} \quad (2)$$

here c is the speed of light, n_c is the critical density, n_e is the electron density at the reflection point of the incident laser, m is the electron mass, M is the ion mass, z is the charge state and $a^2 = I\lambda_\mu^2/(1.37\ x\ 10^{18})$, where I is the laser intensity in W cm^{-2} and λ_μ is the laser wavelength in micrometers. For high intensity laser-matter interactions, the laser pulse continues to propagate up to relativistic critical density [18] and then

$$n_c = n_e/\sqrt{1 + a^2/2} \quad (3)$$

By substituting the expression for n_c into equation 2, we have the following expression for the recession velocity:

$$u_s/c = \sqrt{\tfrac{1}{2}\frac{zm}{M}\frac{a^2}{\sqrt{1+a^2/2}}} \quad (4)$$

At an intensity of 3x10^{18} W/cm^2, the recession velocity (u_s/c) of the accelerated proton is 0.020 and hence the acceleration energy is 0.2 MeV which is very low comparing to the measured one (3.1±0.11 MeV). The most energetic ions can acquire twice the recession velocity as they bouncing in the potential well at the boundary [42]. Then the maximum value of proton recession velocity becomes 0.04 and the maximum acceleration energy becomes 0.75 MeV which is still much lower than the measured one.

Simulation by Sentoku *et al.* [19], has shown that at the laser irradiated target surface, the laser pressure sets an electric field, which sweeps electrons from the interaction region, and induces FSA of ions into and through the target. In the case of long laser pulse, 400-500 fs, the laser pulse continuously pushes the surface by its pressure and the interface is moving during the sweeping acceleration process. In agreement with the simulation, Y. Oishi *et al.* experimentally proved that the maximum proton energy increases as the pulse duration is increased while the laser intensity is kept constant [43]. The sweeping velocity of the accelerated ions is given as [19]:

$$u_{sw}/c = \left[\frac{2m}{M}\left(\sqrt{1+a^2} - 1\right)\right]^{1/2} \quad (5)$$

As a result, the maximum velocity V_{max} of the accelerated ions is given by [19]:

$$V_{max} \approx u_s + 1.5\, u_{sw} \qquad (6)$$

When the irradiance intensity is $3x10^{18}$ W/cm^2, the proton sweeping velocity (u_{sw}/c) is 0.03 and the maximum velocity (V_{max}) is ≈ 0.085. This means that protons can be accelerated due to both radiation pressure and sweeping up to ≈ 3.3 MeV in the laser direction. Thus the experimentally measured value (3.1± 0.11 MeV) could be easily explained. Comparing to metal targets, protons with energies as high as 1.5 MeV have been observed when a laser with the same intensity was focused on an Al target with a thickness of 1.8 mm [16]. PIC simulation [22], gives a value of 25 μm for the thickness above which TNSA protons accelerated from the back surface become less energetic than shock-accelerated protons coming from the front of the target.

To elucidate the observed spectra and to calculate both the total number and the mean energy of the accelerated ions, we performed numerical experiments by using 3-D Monte Carlo code (gray lines in figs 1&2). The code is used to calculate the spectra of neutrons produced by the ^{7}Li (p,n)^{7}Be reaction in a finite thickness target and emitted in specific directions of observation. In the code, accelerated protons having Maxwellian energy distribution interact with the bulk ions inside the target. The time step is taken to be enough for large number of collisions. In addition, the stopping power of the accelerated ions inside the target is taken into account.

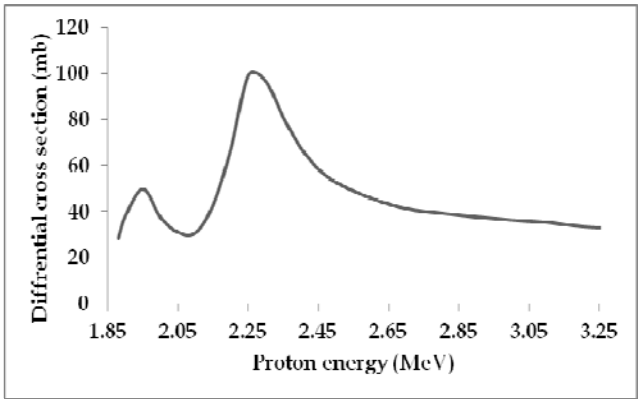

Fig. 3: The differential cross section σ(E, θ) of the ^{7}Li (p,n)^{7}Be reaction at 40 degree. It is clear that the differential cross section shows peaks at certain values of energy which reflects itself in producing neutron peaks in both the measured and calculated neutron spectra.

The neutron yield emitted in a specific direction is calculated using the reaction differential cross-section and its angular distributions referred from experimental and evaluated data [35]. In the calculations, ions are supposed to have anisotropic Maxwellian momentum distribution. The neutron yield is calculated to be the number of neutron emitted per unit solid angle in unit energy interval $d^2N/d\Omega\ dE$ (neutrons/MeV Sr). The measured and calculated neutron spectra include neutron peaks due to the fact that the differential cross section σ(E, θ) of the ^{7}Li (p,n)^{7}Be reaction shows peaks at certain values of energy (Fig. 3) [35]. The neutron spectra observed at 40^0 should have two peaks at 0.15 and 0.55 MeV caused by σ(E, 40^0) that has two peaks at 1.96 and 2.34 MeV for the incident protons.

To check whether or not the model is appropriate, we used the chi-square X^2 as a likelihood estimator. The probability Q=*GAMMQ* (0.5 υ, 0.5 X^2) that gives a quantitative measure for the goodness-of-fit of the model is ≈ 0.13 for LiF and ≈ 0.11 for CH-LiF indicating that the fit is believable [44]. Here *GAMMQ* is the incomplete gamma function and υ is the degree of freedom (the number of data points minus the number of adjustable parameters). In addition, the likely errors of the best fit parameters are determined. The ion mean energy is 430±40 KeV. The total numbers of the accelerated protons are $1.6\pm0.16x10^{13}$ and $6.8\pm0.07x10^{12}$ for the CH-LiF and Li F targets respectively. Protons with a total number of 10^9, much less than here, have been observed when a laser with an intensity of $3x10^{18}$ W/cm^{2}was focused on an Al target [16].

4. Conclusion

In this work, the process of proton acceleration inside plastic and inorganic targets (LiF and CH-LiF) irradiated by an ultra-intense laser at intensity of $3x10^{18}$ W/cm^2 is investigated. The accelerated protons, coming from the CH layer and/or the contaminations on the target, are stopped inside a 500 μm LiF layer. Through the ^{7}Li (p,n) ^{7}Be reaction, the protons are converted to neutrons which readily carry information from inside the target. The TNSA mechanism at the rear side is cancelled and hence we could confirm that the produced protons originate at the irradiated surface and are accelerated inside the target only. The total number of the accelerated protons is much higher than that produced from the metal targets. The maximum acceleration energy can be explained by considering the acceleration due to both the radiation pressure and sweeping into and through the target. Thus the acceleration energy increases with increasing the pulse duration. We found that the measured maximum energy of the accelerated protons is higher than that measured for the protons produced form Al target under the same irradiation conditions. A word remains to be said, under higher irradiation conditions, other neutron producing reactions like photo-nuclear reactions and the reactions of the accelerated protons with ^{6}Li and ^{19}F ions have to be taken into account.

Acknowledgements

We are grateful to the members of the Laser, Target, and measurement Tech. for their technical assistance.

References

[1] M. Roth, T. E. Cowan, M. H. Key et al., Phys. Rev. Lett. **86**, 436 (2001).

[2] J. Raloff, Science News (Washington, D. C.) **156**, 257 (1999).

[3] M. I. K. Santala, M. Zepf, F. N. Beg et al., Appl. Phys. Lett. **78**, 19 (2001).

[4] I. Spencer, K. W. D. Ledingham, R. P. Singhal, T. McCanny, P. McKenna, E. L. Clark, K. Krushelnick, M. Zepf, F. N. Beg, M. Tatarakis, A. E. Dangor, P. A. Norreys, R. J. Clarke, R. M. Allott, and I. N. Ross, Nucl. Instrum. Methods Phys. Res. B **183**, 449 (2001).

[5] D. S. Gemmel, Rev. Mod. Phys. **46**, 129 (1974).

[6] A. J. Mackinnon, P. K. Patel, M. Borghesi, R. C. Clarke, R. R. Freeman, H. Habara, S. P. Hatchett, D. Hey, D. G. Hicks, S. Kar, M. H. Key, J. A. King, K. Lancaster, D. Neely, A. Nikkro, P. A. Norreys, M. M. Notley, T. W. Phillips, L. Romagnani, R. A. Snavely, R. B. Stephens, and R. P. J. Town, Phys. Rev. Lett. **97**, 045001 (2006).

[7] J. M. de Conto, J. Phys. IV (France) **9**, 115 (1999).

[8] V. Y. Bychenkov, V. T. Tikhonchuk, S. V. Tolonnikov et al., Sov. Phys. JETP **88**, 1137 (1999).

[9] K. Lee, J. Y. Lee, S. H. Park, Y.-H. Cha, Y. W. Lee, K. N. Kim, Y. U. Jeong, Phys. Plasmas, **18**, 013101 (2011).

[10] L. Willingale, G. M. Petrov, A. Maksimchuk, J. Davis, R. R. Freeman, T. Matsuoka, C. D. Murphy, V. M. Ovchinnikov, L. Van. Woerkom, K. Krushelnick, Plasma Phys. Control. Fusion, **53,** 014011 (2011).

[11] R. A. Snavely, M. H. Key, S. P. Hatchett, T. E. Cowan, M. Roth, T. W. Phillips, M. A. Stoyer, E. A. Henry, T. C. Sangster, M. S. Singh, S. C. Wilks, A. MacKinnon, A. Offenberger, D. M. Pennington, K. Yasuike, A. B. Langdon, B. F. Lasinski, J. Johnson, M. D. Perry, and E. M. Campbell, Phys. Rev. Lett. **85**, 2945 (2000).

[12] A. J. Mackinnon, M. Borghesi, S. Hatchett, M. H. Key, P. K. Patel, H. Campbell, A. Schiavi, R. Snavely, S. C. Wilks, and O. Willi, Phys. Rev. Lett. **86**, 1769 (2001).

[13] M. Hegelich, S. Karsch, G. Pretzler, D. Habs, K. Witte, W. Guenther, M. Allen, A. Blazevic, J. Fuchs, J. C. Gauthier, M. Geissel, P. Audebert, T. Cowan, M. Roth, Phys. Rev. Lett. **89**, 085002 (2002).

[14] E. L. Clark, K. Krushelnick, J. R. Davies, M. Zepf, M. Tatarakis, F. N. Beg, A. Machacek, P. A. Norreys, M. I. K. Santala, I. Watts, A. E. Dangor, Phys. Rev. Lett. **84**, 670 (2000).

[15] E. L. Clark, K. Krushelnick, M. Zepf, F. N. Beg, M. Tatarakis, A. Machacek, M. I. K. Santala, I. Watts, P. A. Norreys, and A. E. Dangor, Phys. Rev. Lett. **85**, 1654 (2000).

[16] A. Maksimchuk, S. Gu, K. Flippo, D. Umstadter, VY.Bychenkov Phys Rev Lett. **84**, 4108 (2000).

[17] S. C. Wilks, A. B. Langdon, T. E. Cowan, M. Roth, M. Singh, S. Hatchett, M. H. Key, D. Pennington, A. MacKinnon, and R. A. Snavely Phys. Plasmas **8**, 542 (2001).

[18] A. Pukhov, Phys. Rev. Lett. **86**, 3562 (2001).

[19] Y. Sentoku, T. E. Cowan, A. Kemp, H. Ruhl, Phys. Plasmas 10, 2009 (2003).

[20] M. Zepf, E.L. Clark, F.N. Beg, R.J. Clarke, A.E. Dangor, A. Gopal, K. Krushelnick, P.A. Norreys,. M. Tatarakis, U. Wagner, M.S. Wei, Phys. Rev. Lett. **90**, 064801 (2003).

[21] S .Karsch ,S .Diisterer, H. Schwoerer, F. Ewald, D. Habs, M. Hegelich ,G. Pretzler, A. Pukhov, K. Witte, R. Sauerbrey, Phys .Rev. Lett. **91**, 015001 (2003).

[22] Emmanuel d'Humières, Erik Lefebyre, Laurent Gremillet and Victor Malka, Phys. Plasmas **12**, 062704 (2005).

[23] Paul Gibbon, Phys. Rev. E **72**, 026411 (2005).

[24] J. Badziak, S. Glowacz, S. Jablonski, P. Parys, J. Wolowski, H. Hora, J. Krasa, L. Laska, K. Rohlena, Plasma Phys. Controlled Fusion **46**, B541 (2004).

[25] J. Badziak, S. Jablonski, P. Parys, M. Rosinski, J. Wolowski, A. Szydlowski, P. Antici, J. Fuchs, A. Mancic, J. Appl. Phys. **104**, 063310 (2008).

[26] K. Lee, S. H. Park, Y.-H. Cha, J. Y. Lee, Y. W. Lee, K.-H. Yea, and Y. U. Jeong, Phys. Rev. E **78**, 056403 (2008).

[27] K. Lee, J. Y. Lee, Y.-H. Cha, Y. W. Lee, S. H. Park, Y. U. Jeong, Phys. Plasmas **16**, 013106 (2009).

[28] G. Pretzler, A. Saemann, A. Pukhov, T. Scha¨tz, U. Schramm, P. Thirolf, D. Habs, K. Eidmann, G. D. Tsakiris, J. Meyer-ter-Vehn, K. J. Witte, Phys. Rev . E 58, 1165 (1998).

[29] L. Disdier, J-P. Graconnet, G. Malka, J-L. Miquel, Phys. Rev. Lett. 82, 1454 (1999).

[30] D. Hilscher, O. Berndt, M. Enke U. Jahnke, P. V. Nickles, H. Ruhl, and W. Sandner, Phys. Rev. E **64**, 016414 (2001).

[31] N. Izumi, Y. Sentoku, H. Habara et al., Phys. Rev . E **65**, 036413 (2002); H. Habara, R. Kodama, Y. Sentoku et al., Phys. Rev. E **69**, 036407 (2004).

[32] A. Youssef, R.Kodama, H. Habara et al., Phys. Plasmas 12, 110703 (2005); It has been selected by **APS** and **AIP** for J. Ultarfast Science 4(12), High field physics, Dec. (2005).

[33] A. Youssef, R. Kodama, and M. Tampo, Phys. Plasmas 13, 030701 (2006), A. Youssef, R. Kodama, M. Tampo, Phys. Plasmas 13, 030702 (2006).

[34] A. Youssef and R. Kodama, Nucl. Fusion **50**, 035010 (2010), A. Youssef, Phys. Scr. **87**, 015501 (2013).

[35] J. H. Gibbons and H. W. Newson, "H. Liskien et. al, "Neutron production cross- section and energies for reaction ^{7}Li(p,n) ^{7}Be", Nuclear Data Tables, **15**, 57-84, (1975).

[36] Y. Kitagawa, R. Kodama, K. Takahashi et al., Fusion Eng. Des.**44**, 261 (1999).
[37] R. A. Lerche and D. W. Phillion, in Conference Record of the 1991 IEEE Nuclear Science Symposium and Medical Imaging Conference, Vol. I (IEEE, Piscataway, NJ,1991), 91CH3100-5.
[38] R. J. Leeper, J. Chang. IEEE Trans. Nucl. Sci. NS-**29**, 798 (1982).
[39] Glenn F. Knoll, Radiation Detection and Measurement, 2nd ed. (John Wiley & Sons, Inc. New York, 1989).
[40] David Halliday, Introductory Nuclear Physics, 2nd ed. 1955 (John Wiley & Sons, Inc. New York).
[41] S. C. Wilks, W. L. Kruer, M. Tabak, and A. B. Langdon, Phys. Rev. Lett. 69, 1383 (1992).
[42] J. Denavit, Phys. Rev. Lett. **69**, 3052 (1992).
[43] Y. Oishi, T. Nayuki, T. Fujii, Y. Takizawa, X. Wang, T. Yamazaki, K. Nemoto, T. Kayoiji, T. Sekiya, K. Horioka, Y. Okano, Y. Hironaka, K. G. Nakamura, and K. Kondo, A. A. Andreev, Phys. Plasmas **12**, 073102 (2005).
[44] W. H. Press, B. P. Flannery, S. A. Teukolsky, W. T. Vetterling, Numerical Recipes, 2nd ed. (Cambridge University Press, New York, 1987).

*Corresponding author: aeltabal@yahoo.com
a.youssef1968@gmail.com